The International Journal of Advanced Manufacturing Technology (2019) 100:2103–2114
https://doi.org/10.1007/s00170-018-2858-0

ORIGINAL ARTICLE

Endurance tests of a linear peristaltic actuator

João Falcão Carneiro [1,2] · Fernando Gomes de Almeida [1,2] · João Bravo Pinto [2]

Received: 8 May 2018 / Accepted: 4 October 2018 / Published online: 13 October 2018

Abstract
Pneumatic actuators are typically discarded for applications where fine motion control is required, mainly due to the nonlinearities caused by friction effects between piston and rod seals. Conventional control laws are unable to counteract this phenomenon, and thus, conventional actuators find limited applicability in servo control systems. Recently, the use of an alternative solution, a pneumatic linear peristaltic actuator (PLPA), was proposed to overcome this problem. In its present embodiment, a PLPA comprehends two rollers pressing a hose and thereby defining two separate chambers. The use of a PLPA has several potential advantages over conventional or low friction actuators, but its endurance is yet to be known as no studies on this topic can be found in literature. This paper tries to fill this gap by presenting an experimental characterization of some mechanical properties of three different hoses, which are subsequently used in experimental endurance tests. This paper also presents a detailed description of the failure causes found and an analysis on how different parameters may influence its longevity. Finally, possible solutions to increase the life of PLPAs are envisaged.

Keywords Servopneumatic systems · Pneumatic actuators · Motion control · Linear peristaltic actuators

1 Introduction

Pneumatic actuation systems offer inherent advantages such as long service life, high compliance and good power to weight ratios. They also do not exhibit significant thermal or magnetic fields and are therefore good candidates in some specific applications like for instance explosive environments. However, the control of pneumatic systems is typically very complex and often requires model dependant control laws [1–3], due to the nonlinear nature of this type of systems and to the strong influence of friction in their behaviour. Even though attempts have been made towards the development of control laws less dependent on system characteristics (see for instance [4]), the fact is that pneumatic actuated solutions still present strong limitations for fine motion control.

✉ João Falcão Carneiro
jpbrfc@fe.up.pt

Fernando Gomes de Almeida
fga@fe.up.pt

João Bravo Pinto
jbpinto@inegi.up.pt

[1] Faculdade de Engenharia, Universidade do Porto, Rua Dr. Roberto Frias, s/n, 4200-465 Porto, Portugal

[2] INEGI, Universidade do Porto, Rua Dr. Roberto Frias, 400, 4200-465 Porto, Portugal

Despite this scenario, the pneumatic actuator industry has not witnessed a significant change of concepts in the last decades. In fact, although huge advances have been achieved regarding the use of more convenient, environmentally friendly and reliable materials, the basic principle underlying the majority of pneumatic actuators is based on the concept of a piston sliding inside a tube. This solution is simple, economic and compact, but the need of ring type seals in medium to high strokes inevitably leads to undesired friction nonlinear effects that compromise the use of pneumatic actuation when accurate control is a major requirement. Short stroke actuators can be obtained with reduced friction effects either by using flexible chambers [5] or tight production clearances in Airpot type actuators [6]. These options have gained an interesting role in niche applications, but given their limited stroke, the applicability is limited. Furthermore, the use of low friction actuators like the ones used in [7, 8] typically leads to the need of coupling the actuator with a mechanical guide to be able to cope with external loads. When this happens, the mechanical alignment between actuator and guide becomes a crucial factor in order to maintain low friction forces on the overall system. A compromise between precise mechanical design to ensure low friction and production cost then becomes a difficult to solve issue. A different approach lies on the use of air bearings in the piston and the rod to eliminate mechanical friction, as explored in [9, 10]. Despite efficiently removing friction effects, this approach leads to complex and expensive solutions, both in acquisition and running costs.

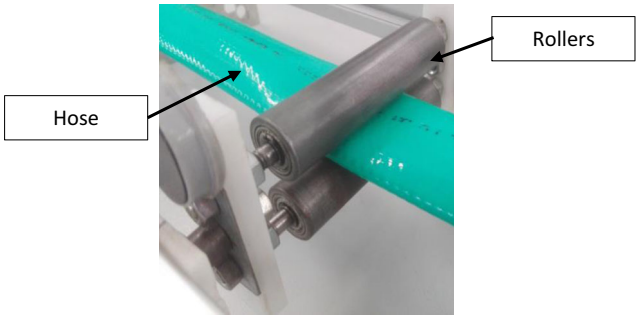

Fig. 1 Pneumatic linear peristaltic actuator

Alternative solutions to conventional piston type actuators can be found in pneumatic artificial muscles (PAMs) and soft rubber actuators. Soft rubber actuators are a recent trend in the pneumatic field [11] and present several advantages like for instance the ability to adapt to the environment, the flexibility on the choice of the actuator shape and their inherent safety in human cooperation activities. For instance, in [12], a humanoid soft robotic hand with a new tube-distribution structure was developed. The proposed structure allows for independent control of each joint whilst reducing the resistance of the fingers bend. Another interesting aspect of [12] lies in the fact that it can be controlled based on surface electromyographic signals measured in the hand of a human master. In [13], several parameters of a circular bellows pneumatic soft actuator were characterized and tested with different silicone materials. The impact of those parameters in the performance of the actuator, namely in the output bending motion and average bending force, according to the applied pressure, was determined. One shortcoming of soft robots lies in the fact that both strokes and forces exhibited by this type of actuators are typically much lower than ones of their piston like counterparts. In order to circumvent, at least partially, these limitations, in [14], a different approach was followed, based on an architecture of several parallel coupled lower power actuators. This architecture takes advantage of the fact that parallel actuator grouping is advantageous over a geometrically equivalent single actuator as it allows the development of more force. Besides that, parallel structures offer robustness against failure of their individual components. In [14], these actuators are tested in a soft actuated platform with closed loop position control. Trajectory following results shows that the control performance is not very accurate, but interesting robustness to unit failures is achieved. Control performance limitations are in fact one of the reasons why at the present moment, soft robots can only be found in very specific applications. Their wide application in industry is thus far from being a reality. Regarding PAMs, it is a very interesting solution regarding friction, because they operate stick-slip-free. However, their highly nonlinear behaviour often results in the need for complex control algorithms [15] just as pneumatic cylinders do [16]. In [17], a comparison is made between an actuator system driven by two PAMs and the same system driven by a conventional pneumatic actuator. Both assemblies were controlled by a sliding mode controller (SMC) and by a sliding mode controller with integral action

Fig. 2 Forces acting in a PLPA

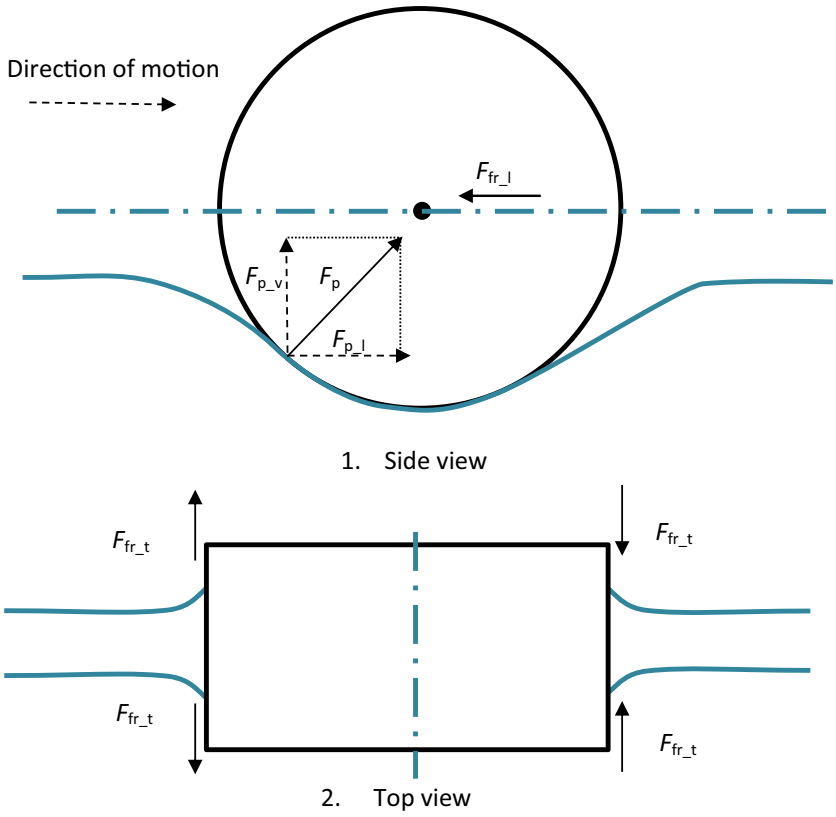

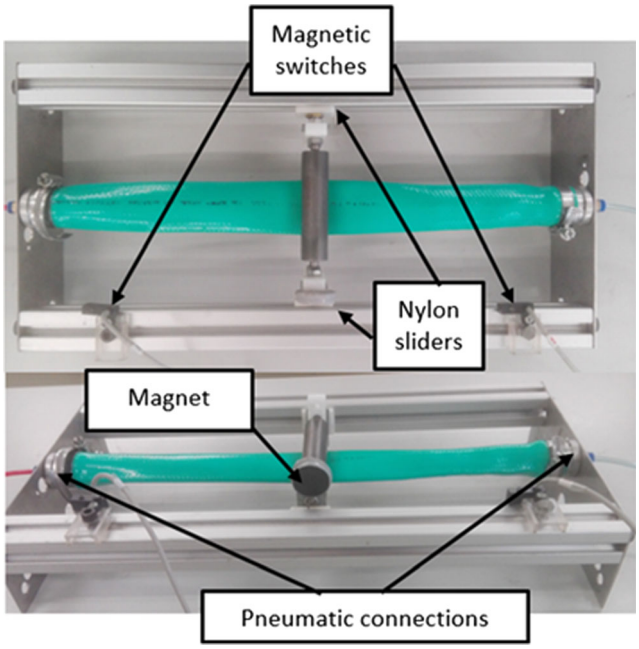

Fig. 3 Experimental setup

(SMCI). The system driven by the pneumatic muscles outperformed the cylinder driven one, in terms of steady-state errors and low-frequency tracking due to its stick-slip-free operation. Despite this advantage, the achievable displacement of this kind of actuators, typically 25 to 30% of the dilated length [18], limits their applicability in industrial applications. In recent years, efforts have been made with the objective of increasing the achievable displacement of pneumatic muscles, such as the development of an inverse pneumatic artificial muscle (IPAM) [19]. By using an elastic latex tube with inextensible fibres wrapped around it to stop radial expansion, a strain of over 300% was achieved. However, just as with PAM's, the IPAM is only active in one way of displacement, whereas the return is achieved through the material's elasticity or other external means.

Another way to reduce the negative friction effects on the system control is to combine electrical and pneumatic actuators [20, 21]. While this kind of solution can outperform conventional pneumatic actuators, regarding steady-state error and reference tracking, it may lead to bulky and/or expensive devices, due to the increase in required equipment. In addition to control difficulties, friction also introduces wear between the contact surfaces, reducing service life of the system. As such, in [22], the contact pressure distribution in guide bearings for pneumatic actuators was investigated and a few design changes to redistribute the contact pressure, improve durability, and reduce wear were suggested. Although friction is a major problem in servopneumatic systems, other phenomena can also degrade their performance, like the air leakage in the actuator seals. This is a very important topic due to energy concerns, and several studies in literature focus on it. For instance, in [23], the air leakage in rodless cylinders with longitudinal slot and sealing band was studied. That study revealed that sharp-edged lip seals were particularly effective on limiting leakage flow rate. The air leakage on the actuator is also of vital importance as it influences the servopneumatic system proprieties, namely around the central position of the servovalve spool.

Table 1 Shore A hardness and Young's modulus

Hose	Internal wall		External wall	
	Shore A	Young's modulus [29] (MPa)	Shore A	Young's modulus [29] (MPa)
FTS	81.6	10.4	82	10.6
HFL	82.8	11.2	82.1	10.7
FGA	74.6	6.9	71.4	5.9

The search for different ways to deal with friction led the authors to develop a pneumatic linear peristaltic actuator (PLPA) in [24, 25]. The PLPA solution envisaged in [24, 25] presented several advantages over conventional or low friction actuators, for both conventional and servo applications. Studies [24, 25] were focused on studying several experimental characteristics of PLPA actuators, like the performance obtained under conventional velocity control, forces obtained, friction characteristics and servocontrol behaviour. In fact, in those studies, it was shown that a PLPA has favourable friction characteristics as it does not present a sharp nonlinear nature. As experimentally shown in [25], this means that very low velocities can be reached without the stick slip phenomenon, contrary to what happens when an Airpot actuator is used. Also, the PLPA allows the achievement of very accurate motion control even when simple control laws are used. In [25], a simple PID type controller was tested in position control using both actuators: whilst a limit cycle occurred with the Airpot actuator, zero steady state error was reached using the PLPA.

Despite its potential, PLPA actuators are prone to suffer high mechanical stress given the need to compress the hose between the rollers to achieve good sealing performance. This was one of the findings of studies [24, 25]. Since, as far as the authors'

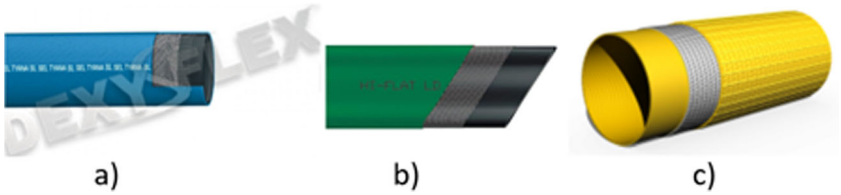

Fig. 4 Types of hose tested. **a** FTS [26]. **b** HFL [27]. **c** FGA [28]

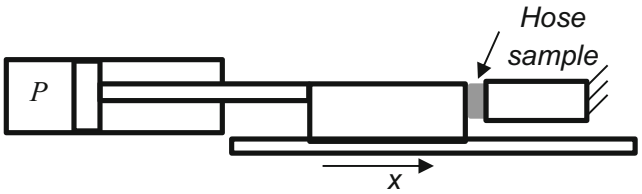

Fig. 5 Experimental setup used to determine the Young modulus of the hoses

knowledge goes, no previous publication has focused on this topic, this paper explores the longevity of PLPA actuators by presenting results that compare the endurance behaviour of three different types of hoses. This not only allows the assessment of the longevity of the solution envisaged in [24, 25] but also, and more importantly, to experimentally determine the main causes of failure. It is therefore expected that this study forms the basis for future work to focus on how to reduce those failure causes. As far as the authors' knowledge goes, this is the first study on this topic.

In the next section, the PLPA working principle is presented, along with an experimental characterisation of the PLPA experimental setup used throughout this work. Section 3 briefly presents the endurance test performed and Section 4 the main results obtained. Section 5 resumes the major conclusions drawn from this work.

2 Pneumatic linear peristaltic actuator

2.1 Working principle

Figure 1 shows the linear peristaltic actuator as initially proposed by the authors in [24]. The assembly is comprised of a hose, pressed between two rollers and hence divided into two chambers. By feeding the hose with compressed air, the pressure difference between the two chambers generates a force (F_p) that acts on the

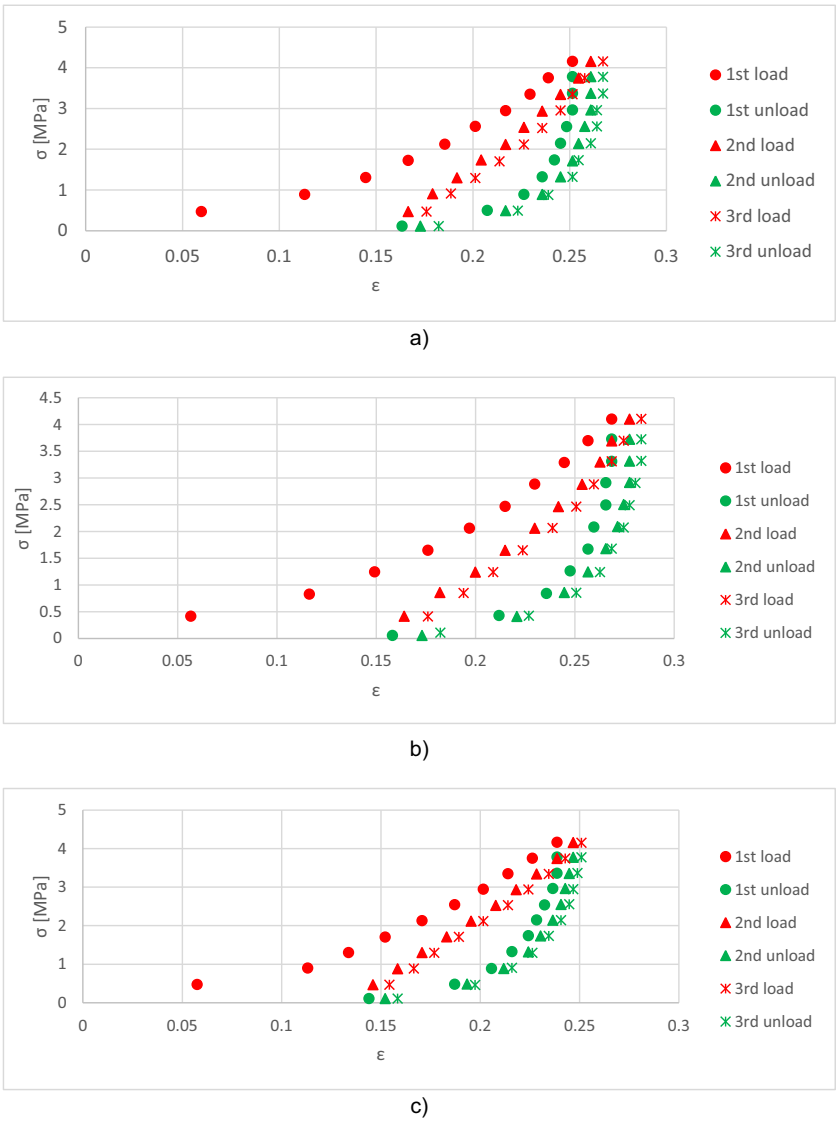

Fig. 6 σ versus ε results. **a** FTS. **b** HFL. **c** FGA

rollers. This force can be projected into its vertical and longitudinal components (F_{p_v} and F_{p_l}, respectively), as shown in Fig. 2.

The vertical component is absorbed by the roller supports, whilst the longitudinal component drives the motion of the rollers. Along the motion direction, only rolling resistance occurs in the actuator [24] due to the ball bearings friction on the rollers (F_{fr_l}). In Fig. 2, it is also represented the sliding friction (F_{fr_t}), which occurs in the transversal direction. This is a dissipative force and, therefore, undesirable for it causes loss of energy. Its effects on motion are expected to be negligible though, as its direction is mostly perpendicular to the direction of motion. Each roller support is connected to a slider which runs in a T-slot aluminium profile and guides the PLPA. As such, in this particular setup, there is sliding friction between the sliders and the profiles. This sliding resistance, however, is not represented in Fig. 2 as it depends on the guidance solution for the PLPA. In the present study, the existence of sliding friction in the guidance system is not critical because this setup is only used for longevity assessment. For servo control, it is recommended that a guidance system without sliding friction is adopted, like for instance the one used in [24, 25]. Finally, the reader is referred to [24, 25] for more information on the characteristics of PLPA, namely regarding the forces developed, the motion accuracy performance and the velocities obtained experimentally by these type of actuators.

2.2 Experimental setup and hose characterization

The setup used to perform the endurance tests is shown in Fig. 3. It comprises a PLPA with two sliders on each end, which run in two T-slot aluminium profiles. On each end of one of the profiles, there is a magnetic switch activated when a magnet attached to the PLPA approaches. The useful stroke of the actuator is determined by the magnetic switches position. In this study, the useful stroke is 284 mm (a maximum of 300 mm can be adjusted). The hose length is ca. 400 mm. The rollers are made of steel, have an external diameter of 20 mm and include ball bearings to reduce friction. The setup also includes two pressure transducers manufactured by Druck (model PTX 1400) with a range between 0 and 10 bar, a mass flow meter manufactured by Teledyne Hastings Instruments (model HFM-201) with a range between 0 and 100 slpm (standard litre per minute), a 5/2 electrically operated directional valve, two magnetic switches, two quick exhaust valves and a counter. The pressure transducers and the mass flow meter are connected to the PLPA to perform leakage measurements, as described in Section 3.2.

The choice of the hoses tested in this work was based on three requisites: the hose should not be expensive; it should withstand six bars of pressure and still be flexible enough to be easily accommodated between the PLPA rollers. Based on these criteria, three types of hoses, shown in Fig. 4, were found and tested. The first one (Fire TYANA SL—FTS) is manufactured by Dexyflex and includes three layers: an inner

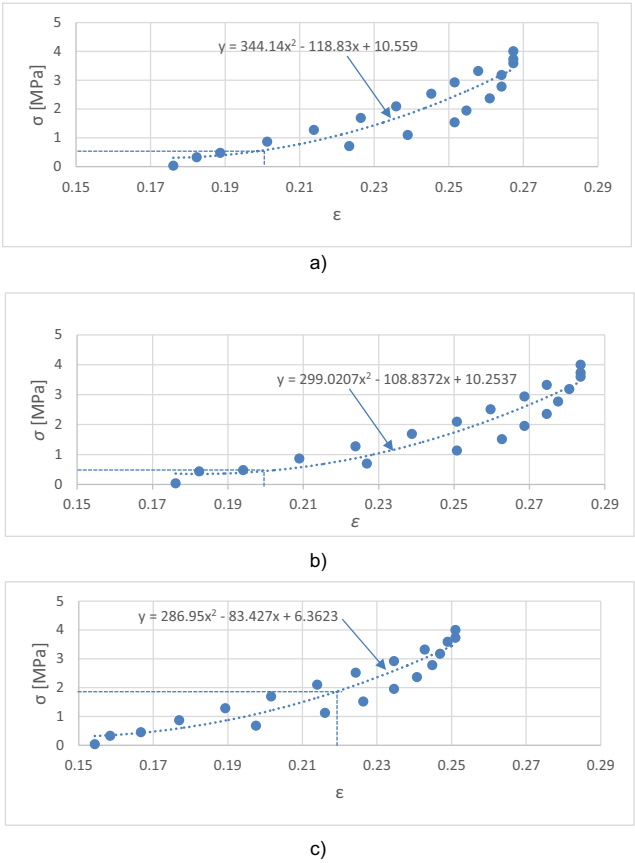

Fig. 7 σ versus ε results, friction compensated, for the 3rd load-unload cycle. **a** FTS. **b** HFL. **c** FGA

flexible PVC linen, a high tensile synthetic textile reinforcement and an outer weather resistant PVC. This hose is typically used for light discharge of water in agriculture and industry. It has a working pressure of 5 bar and burst pressure of 14 bar. The price of this hose for the end consumer is around 1 euro/m. The second hose tested (HIFLAT LD—HFL) is manufactured by FITT and is composed by PVC with a textile reinforcement. According to the information provided by the manufacturer, it is suitable in agriculture for light duty purposes at medium and high temperature usage. The working pressure is 6 bar, and the burst pressure is 18 bar. The price of

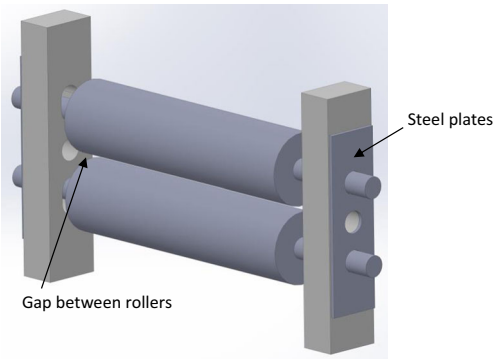

Fig. 8 Mechanical solution to impose distance between rollers

Table 2 Relevant dimensions for each hose

Hose	Thickness, ϵ_0 (mm)	Gap between rollers (mm)	Strain, ε (%)
FTS	1.54	2.47	19.97
HFL	1.54	2.47	19.97
FGA	2.31	3.62	21.75

this hose was around 1.5 euro/m. The third type of hose tested (FLEXIGOM AIR—FGA) is manufactured by Productos Mesa. This hose is composed by a flexible nitrile rubber sleeve with internal textile fabric and an abrasion resistant external coating. Its reinforced middle textile is made from high tenacity polyester thread. This hose is specifically designed for use with compressed air and has a working pressure of 30 bar, whereas its burst pressure is superior to 90 bar. Given the extra pressure accommodation, this hose is the most expensive one, with an end consumer price around 9 euros/m.

In order to mechanically characterize the hoses, shore A hardness tests were performed on each hose type using a durometer test machine Sauter HBA 100-0. For each hose, ten measurements were performed in the internal and external walls. Table 1 presents the average of those experiments.

The Young modulus of the hoses is not available in the manufacturer's datasheet but can be estimated based on the indentation values, as presented in [29]. Table 1 also presents the Young modulus results obtained using this approach. In order to validate these values and to determine the stress undergone by each hose in the longevity trials, compression tests were performed, using a conventional pneumatic cylinder to compress a sample of each hose against a fixed wall—see Fig. 5.

For each hose, three load/unload cycles were performed, whilst acquiring the pressure (P) inside the working chamber and the piston displacement x. The strain ε and stress σ that each hose sample was subject to were then calculated using Eqs. (1) and (2)

$$\varepsilon = \Delta x / \epsilon_0 \tag{1}$$

$$\sigma = F_{\text{pneu}} / A_{\text{sample}} \tag{2}$$

where Δx is the change in the piston position, A_{sample} is the area of the hose sample, ϵ_0 is the hose thickness and F_{pneu} is the pneumatic force exerted by the piston due to pressure P. It should be noted that the calculation of strain ε and stress σ using (1) and (2) neglects friction static forces in the piston of the pneumatic cylinder. As shown in [30], these static friction forces in systems comprising pneumatic cylinders are very hard to determine and exhibit considerable uncertainty as they depend on temperature, previous load history, working pressures, etc. For the particular system used in this work, it was found in [30] that static friction forces range from ca. 27 to 38 N. Consequently, for small values of σ, results must be carefully analyzed as they do not take into account friction effects. This effect can nonetheless be compensated, as will be shown later in this section.

The results obtained with this procedure are shown in Fig. 6. Three effects should be underlined: first, a significant hysteresis behaviour is noticed, and second, a significant strain hardening effect is seen from the first to the second load-unload cycle. Third, this hardening effect significantly diminishes from the second to the third cycle, suggesting that further load-unload cycles do not lead to significant changes.

Consequently, the 3rd load-unload cycle will be used as a reference for further analysis. In order to take into account the static friction effects on the system, the stress caused by the maximum static friction force [30] was compensated on each sample of F_{pneu}. Since the ultimate goal of these curves is to estimate the stress the hose is subject to for a given roller distance (please cf. the end of this section), and since in normal use the hose can either be under load or unload effort, a single curve was fit to loading and unloading data. Results from this exercise are presented in Fig. 7 and will be used as indicative values of the stress undergone by each hose for a given strain. It should be underlined that the results presented in Fig. 7 indicate a Young modulus range that includes the values in Table 1, thereby validating the order of magnitude of the estimates calculated using the procedure presented in [29].

In order to ensure that leakage between chambers is within acceptable values, the distance between rollers is mechanically

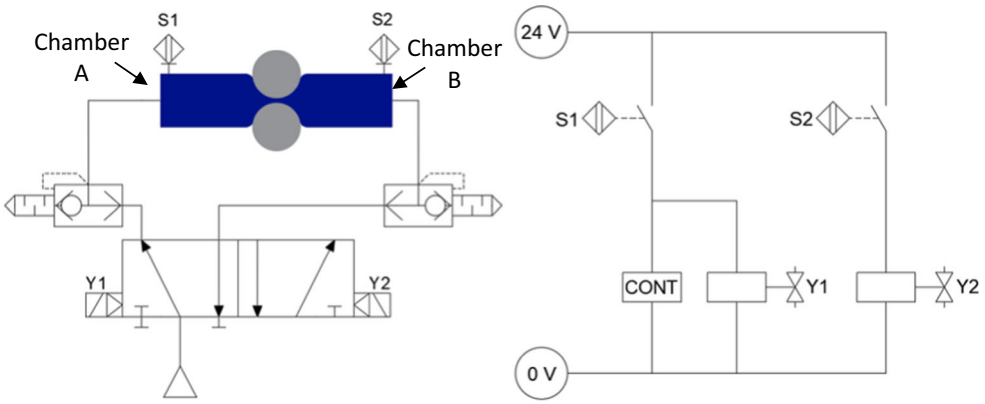

Fig. 9 Pneumatic and electric schematics for the endurance tests

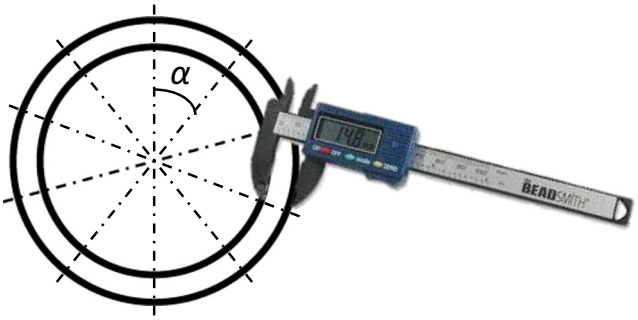

Fig. 10 Measurement of hose thickness

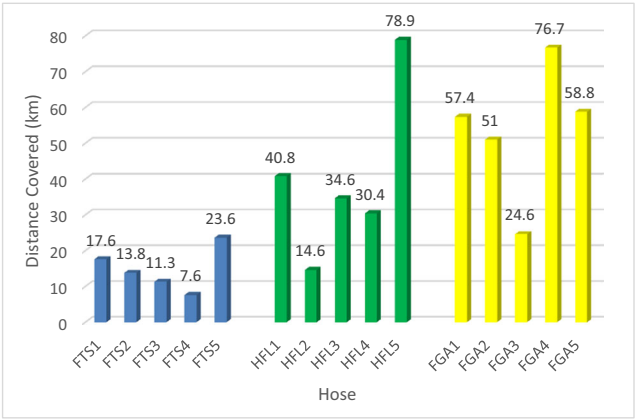

Fig. 12 Hose travel distance

imposed. This distance was adjusted using steel plates with holes to fit the rollers' axis, as detailed in Fig. 8. The distance between rollers was determined in trial and error based experiments. These trials were performed up until a compromise between good sealing, on the one hand, and a limited hose compressive pressure, on the other, was achieved. Two sets of plates were made: one for FTS and HFL, as they have the same thickness, and one for the FGA hose. Table 2 presents some relevant dimensions for each hose.

Using the geometrical values presented in Table 2 and the curves fitted in Fig. 7, it can be seen that the stress of the FTS and HFL hoses is ca. 0.5 MPa, whilst for the FGA hose, this value is approximately 1.8 MPa.

These values indicate that the hoses will be able to withstand pressures from ca. 5 bar to ca. 18 bar without leakage. It should be stressed that these are only indicative values, due to uncertainty both in static friction effects and geometrical measurements. In addition, the above-mentioned values are determined using average calculations of load and unload cycles, but a significant variation exists between both cycles. Despite these limitations, the values presented above provide a rough estimate showing that the order of magnitude of the stress imposed on the hose is within the values of compressed air pressure used in conventional pneumatics.

3 Description of the endurance tests

The pneumatic assembly and the electric circuit used to carry out the endurance tests are presented in Fig. 9. The magnetic switches S1 and S2 activate solenoids Y1 and Y2 of the directional valve, so that the rollers move back and forth. The counter (CONT) is activated by magnetic switch S1. The endurance tests were carried out at a source pressure $P_s = 3$ bar. A test was considered to be over when the hose presented visible signs of failure, i.e. when it tore or when small holes appeared.

Since the sealing between chambers is achieved by pressing the hose between the rollers, the hose thickness was measured before and after the endurance tests, as described in detail in Section 3.1. Also, leakage measurements were performed to one of each type of hose tested. The leakage measurements are detailed in Section 3.2.

3.1 Thickness measurements

For each hose tested, ten thickness measurements were taken before and after the endurance test was performed. Measurements

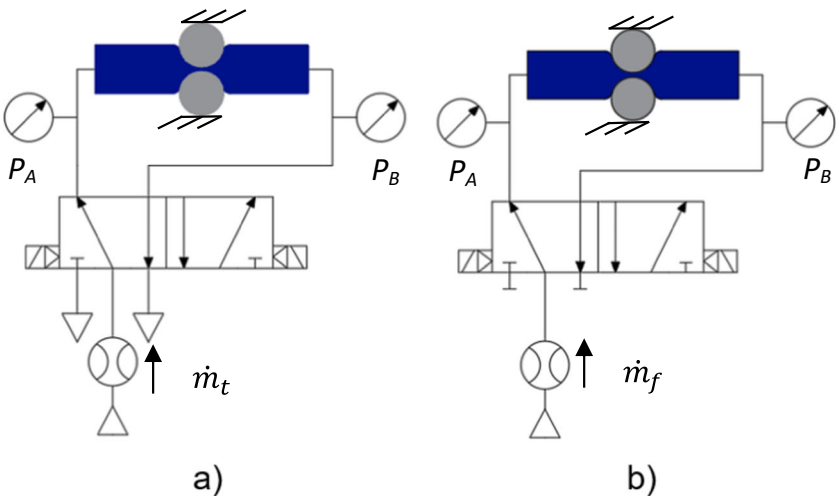

Fig. 11 Schematic of the assemblies for the leakage measurements—example for chamber A measurements

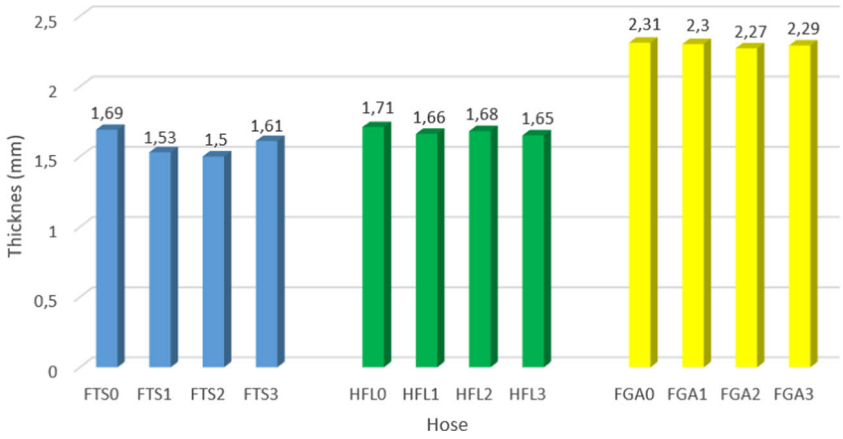

Fig. 13 Hose average thickness reduction

taken after the endurance test were performed in regions of the hose that had undergone the rollers' load. A digital caliper with 0.01-mm resolution was used. The measurements were taken at equal angular intervals $\alpha = 36°$ around each hose perimeter, as exemplified in Fig. 10. The average of the ten measurements was then considered for comparison.

3.2 Leakage measurements

The leakage measurements were performed in two experiments. In the first experiment, the total leakage $\dot{m}_t$ (e.g. between chambers, through the pneumatic fittings) was determined by mechanically blocking the rollers at the middle of the actuators length and pressurizing one chamber whilst leaving the other open, as shown in Fig. 11a). Leakage measurements were performed in both chambers A and B. The leakage was determined for pressure values (P_A and P_B, please check Fig. 9) ranging from 1 to 6 bar, using 1 bar steps. The second experiment was identical to the first one, with the exception of being carried out with the nonpressurized chamber closed (see Fig. 11b)). This assembly allowed for the leakage flow between the pneumatic fittings and the atmosphere ($\dot{m}_f$) to be determined. The difference between the flow values in each experiment allows the determination of the inter-chamber leakage ($\dot{m}_i$), as shown in equation (3):

$$\dot{m}_i = \dot{m}_t - \dot{m}_f \tag{3}$$

4 Experimental results

4.1 Distance covered

Several samples of each type of hose were subjected to endurance tests. Five representative samples of each type were chosen for analysis: 5 FTS hoses (FTS1 to FTS5), 5 HFL hoses (HFL1 to HFL5) and 5 FGA hoses (FGA1 to FGA5). The distance covered by each hose is shown in Fig. 12.

The FGA hoses covered the biggest distance with an average of 53.7 km, followed by the HFL hoses with 39.9 km, leaving behind the FTS hoses, which covered 14.8 km in average.

4.2 Thickness reduction

Due to the sealing being achieved through the pressing of the hose between the rollers, the thickness of each hose was measured,

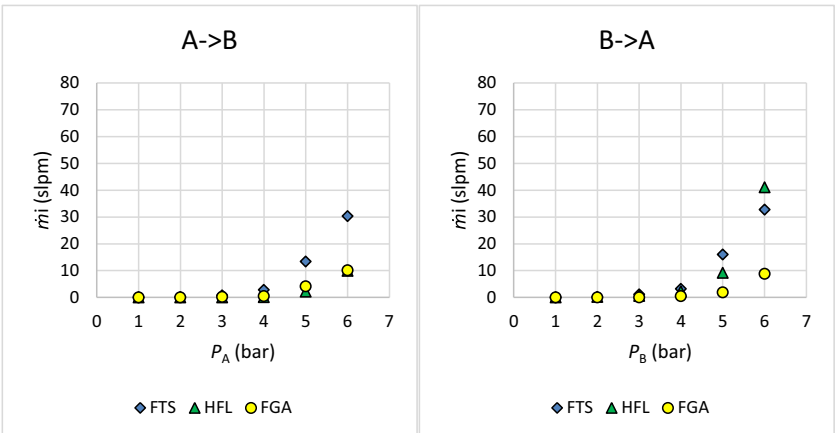

Fig. 14 Leakage measurements at M_1

using the procedure presented in Section 3.1, after the endurance tests took place. The results of this comparison are illustrated in Fig. 13, which also presents the average thickness results obtained with a nontested hose sample (hose xxx0), for datum purposes. It should be underlined that the average thickness obtained for hoses FTS and HFL is slightly higher than the one measured in the samples of the compression tests of Section 2.2 (ϵ_0). This is caused by an irregular thickness of the hose around its perimeter.

By analyzing the results presented in Fig. 13, it becomes clear that there is a consistent permanent thickness reduction of the hoses. This result was observed on all hoses, but it is clearer on the FTS type than on the HFL or the FGA. In fact, the FTS thickness reduction reaches a maximum value around 11.5%, whilst on the HFL, the maximum thickness reduction is 3.5% and on the FGA is around 2%. This thickness reduction will lead to a change in the hoses sealing capability, as will be seen in the next section.

4.3 Leakage between chambers

Leakage measurements were carried out to one hose of each type. Measurements were taken in two distinct moments: one before the endurance trials begun (M_1) and one at about one half of the service life of the least-lasting hose (M_2). Figures 14, 15 show the inter-chamber leakage mass flow $\dot{m}_i$ from chambers A to B and vice versa, at M_1 and M_2, respectively.

Figures 14, 15 clearly reveal an increase in leakage with the increase of pressure. In addition, with the exception of the FGA hoses, for each pressure level, there is a consistent leakage increase with wear. It should be noted that in Fig. 15, there are no values for the HFL hose leakage at M_2 and 6 bar, as it exceeded the flowmeter range.

4.4 Hose failure

Pictures were taken to record the state of the hoses after each endurance test. Figures 16, 17, 18 show the location of the hose failure on one hose of each type.

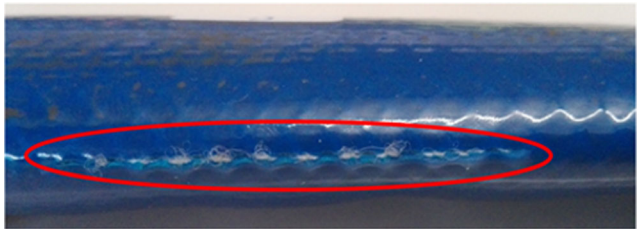

Fig. 16 Failure in hose FTS3

A pattern was identified when it came to the location of the failure: every hose failed in the folding region. A clear tearing is visible in hoses FTS3 and FGA2 (see Figs. 16, 18), whilst small elliptic shaped holes appeared in the case of hose HFL1 (see Fig. 17). These holes have an average length of 1.55 mm and an average width of 0.1 mm (see Fig. 19). It should be underlined that similar results were obtained for the other two tested hoses of each type.

4.5 Discussion of results

Endurance tests revealed that, among the different hose types tested, the FGA hoses are the ones exhibiting longer service life. In fact, the FGA hoses allowed the higher distance travelled, with an average of 53.7 km when compared to 39.9 km of the HFL hoses and the 14.8 km of the FTS hoses. This suggests that nitrile rubber may be a kind of material better suited for this type of application when compared to PVC. Another possible justification to this big difference lies on the mechanical wear resistance of the internal textile mesh used in FGA hose. Since this hose withstands higher pressures, its textile mesh should exhibit better mechanical proprieties and hence present higher service life when compared to HFL and FTS hoses. The FGA and HFL hoses are therefore the most appropriate for this application, and the choice among them will necessarily have to take into account economical aspects. In fact, the FGA exhibits longer service life but at a considerable higher cost. However, since FGA hoses are expected to require less maintenance, the machine downtime using FGA hoses is also significantly lower. This

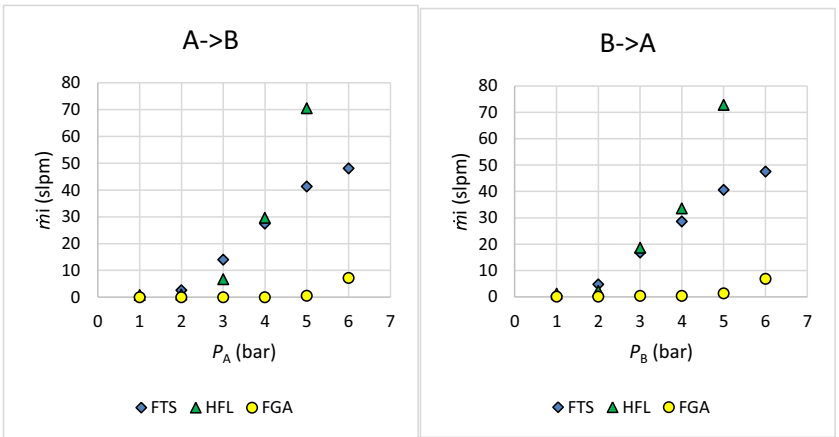

Fig. 15 Leakage measurements at M_2

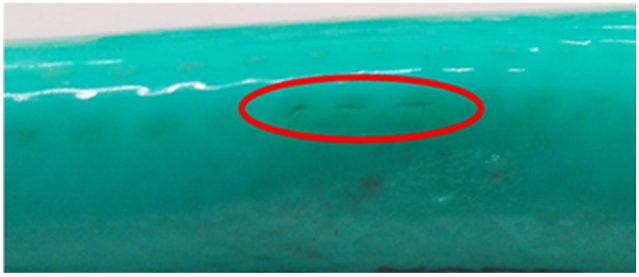

Fig. 17 Failure in hose HFL1

topic falls outside the scope of this paper and will be subject of future studies. Another relevant result obtained in the endurance tests has to do with the substantial dispersion of results. In fact, even under the same experimental conditions, the endurance of the hoses can vary significantly. The causes for such high difference on the longevity are unknown. Possible causes such as defects on the hose and minor differences in the hose stretching will be the topic of future works.

Measurements showed that there is a reduction in hose thickness with wear. This thickness reduction is especially significant in the FTS hoses, with a maximum value of 11.5%. This effect is the least prominent in the FGA hoses whose maximum reduction was 2%. Two factors appear to contribute to the difference between leakage evolutions in the endurance tests: on one hand, FTS and HFL thickness reduction was higher than that of FGA hose. Indeed, since the experimental setup used in this work imposes a distance between rollers, a reduction in the hose thickness leads to a bigger area through which the air can migrate from one chamber to the other. On the other hand, initial stress values imposed in FTS and HFL hoses are significantly lower than that of the FGA hose, leading to lower contact pressures and hence lower sealing capabilities. In this regard, it is also interesting to notice that the hose with higher stress imposed by the rollers is nevertheless the one with higher service life, again suggesting that the type of material of the hose is of utmost importance. Leakage was also shown to increase with inner pressure. This is an expected result, as a higher inner pressure results in a bigger force pushing the hose against the rollers, reducing the contact pressure between hose inner walls.

The consistent location for the hose failure suggests that the hose crease is subject to a lot of strain. As mentioned in Section 2.2, sealing between chambers is achieved by imposing

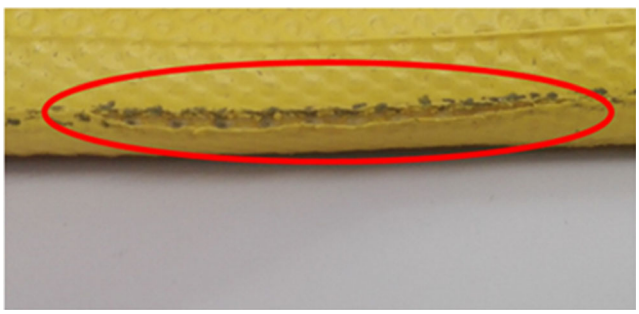

Fig. 18 Failure in hose FGA2

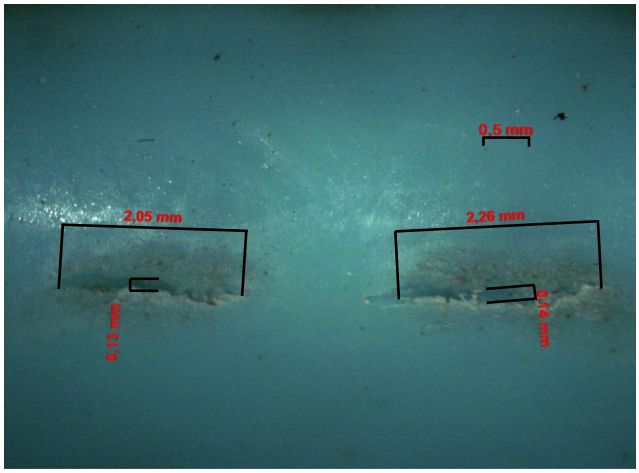

Fig. 19 Picture of holes found in hose HFL1

a fixed distance between the rollers. The motion of the rollers back and forth forces the hose cross section to consecutively unfold and fold, whenever there is compressed air inside it (see Fig. 20a)) and when the rollers pass (see Fig. 20b)), respectively. As a result, the hose is subject to a lot of mechanical strain, eventually tearing due to fatigue.

Finally, it should be noted that the endurance tests revealed a big dispersion of results in the travelled distance. In fact, the ratios between the minimum and maximum distance for each are ca. 64%, 36% and 43% for FTS, HFL and FGA hoses, respectively. This fact, along with the short travelled distance of the PLPA actuator when compared with conventional actuators (tens of kilometres for the PLPA, thousands of kilometres for conventional actuators [31, 32]), does not allow this solution to be applied in an industrial environment at its present state.

There are, nevertheless, important findings from this work that might be applied in future developments. As previously mentioned, the main cause of failure is the tear of the folding part of the hose. This might be overcome if, by mechanical design of the PLPA, the hose does not have to fold completely. Furthermore, it was shown that imposing a fixed distance between the rollers might compromise inter-chamber leakage as the hose wall thickness tends to be reduced with time. This might be surpassed if, again by mechanical design of the PLPA, the force between the rollers—instead of the distance—is imposed.

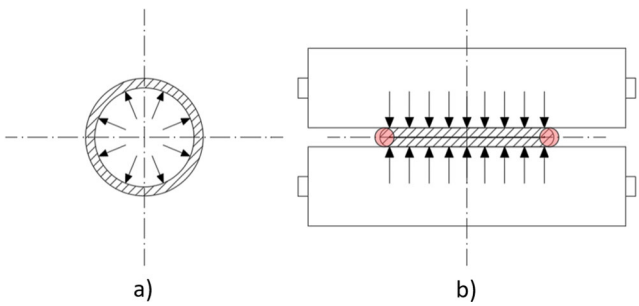

Fig. 20 Hose cross section. **a** With internal air pressure. **b** Pressed by the rollers

5 Conclusion

In this paper, the service life of a pneumatic linear peristaltic actuator was studied. Endurance tests were performed to several samples of three different types of hoses. It was determined that, with the PLPA implementation used in this work, the service life of this kind of actuators is two orders of magnitude lower than the typical service life of conventional pneumatic cylinders. Also, it was shown that the thickness of the hose walls might be significantly reduced during operation. Consequently, since the distance between rollers is imposed, the inter-chamber leakage increases due to this effect. Analysis of the failure sections revealed that the hose folding region was the usual location for hose failure. This work thus allowed the identification of four important issues. First, the mechanism should prevent the hose from completely folding, so that the mechanical strain to which it is subject becomes reduced. Second, future PLPA mechanical design should impose the force between rollers—as opposed to imposing distance—to prevent that a decrease in the hose thickness leads to an increase in the inter-chamber leakage. Third, it was found that the hose with higher stress imposed by the rollers was nevertheless the one with higher service life, suggesting that the material of the hose is of utmost importance. Fourth, a significant dispersion of results on the hose longevity was noticed, even under the same experimental conditions. Future works should therefore explore the causes of such differences. Based on the results obtained in this study, the nitrile rubber based hose (FGA) presents higher longevity than the PVC hoses. This means that lower downtimes for maintenance operations are expected when using FGA hoses. However, the FGA hose used in this study is significantly more expensive than the PVC ones, so an assessment of the best solution from an economical perspective is an interesting topic to be investigated in future work.

Funding information This work is financially support by 'Fundação para a Ciência e a Tecnologia', through contract LAETA—UID/SEM/50022/2013.

References

1. Falcão Carneiro J, Gomes de Almeida F (2014) Micro tracking and positioning using off-the-shelf servopneumatics. Robot Comput Integr Manuf 30(3):244–255
2. Falcão Carneiro J, Gomes Almeida F (2016) On the influence of velocity and acceleration estimators on a servopneumatic system behaviour. IEEE Access 4:6541–6553
3. Falcão Carneiro J, Gomes de Almeida F (2012) A macro-micro motion servopneumatic device. Proc of the Inst of Mech Eng, Part I, J of Syst and Cont Eng 226(6):775–786
4. Falcão Carneiro J, Gomes de Almeida F (2014) Accurate motion control of a servopneumatic system using integral sliding mode control. Int J Adv Manuf Technol 77(9):1533–1548
5. Inc., C. *Rolling diaphragm cylinders*. [cited 20/04/2018]; Available from: https://www.controlair.com/index.php/products/diaphragm-air-cylinders/rolling-diaphragm-cylinders
6. Airpot Corporation. *Pneumatic actuators*. [cited 30/04/2018]; Available from: http://airpot.com/product-category/product-lines/pneumatic-actuation/
7. Yung-Tien L, Tien-Tsai K, Kuo-Ming C, Sheng-Yuan C (2013) Observer-based adaptive sliding mode control for pneumatic servo system. Precis Eng 37(3):522–530
8. Taheri B, Case D, and Richer E (2012) Design of robust nonlinear force and stiffness controller for pneumatic actuators. in 51st IEEE Conference on Decision and Control (CDC). Maui, Hawaii, USA
9. Kagawa T, Tokashiki L, Fujita T (2000) Accurate positioning of a pneumatic servosystem with air bearings. in Proc. of the Bath Workshop on Power Transmis. and Motion Control. ,Bath, UK
10. Li J, Kawashima K, Kagawa T, Fujita T (2011) Trajectory control of pneumatic servo table with air bearing in 2011 International Conference on Fluid Power and Mechatronics. Beijing, China
11. Carmel M (2013) Soft robotics: a perspective—current trends and prospects for the future. Soft Robotics (SoRo) 1(1):5–11
12. Feng N, Shi Q, Wang H, Gong J, Liu C, Lu Z (2018) A soft robotic hand: design, analysis, sEMG control, and experiment. Int J Adv Manuf Technol 97(1–4):319–333
13. Rehman T, Faudzi A, Dewi D, Ali M (2017) Design, characterization, and manufacturing of circular bellows pneumatic soft actuator. Int J Adv Manuf Technol 93(9–12):4295–4304
14. Robertson M, Sadeghi H, Florez J, Paik J (2017) Soft pneumatic actuator fascicles for high force and reliability. Soft Robotics (SoRo) 4(1):23–32
15. Robinson RM, Kothera CS, Sanner RM, Wereley NM (2016) Nonlinear control of robotic manipulators driven by pneumatic artificial muscles. IEEE/ASME Trans on Mechatronics 21(1):55–68
16. Bone GM, Ning S (2007) Experimental comparison of position tracking control algorithms for pneumatic cylinder actuators. IEEE/ASME Trans on Mechatronics 12(5):557–561
17. Jouppila, V., S. Andrew Gadsden, and A. Ellman, Experimental comparisons of sliding mode controlled pneumatic muscle and cylinder actuators. J Dyn Syst Meas Control, 2014. 136(4): p. 044503–044503–10
18. Krivts I, Krejnin G (2006) Pneumatic actuating systems for automatic equipment: structure and design. CRC Press, Boca Raton
19. Hawkes EW, Christensen DL, Okamura AM (2016) Design and implementation of a 300% strain soft artificial muscle. in 2016 IEEE International Conference on Robotics and Automation (ICRA)
20. Bone G, Xue M, Flett J (2015) Position control of hybrid pneumatic–electric actuators using discrete-valued model-predictive control. Mechatronics 25:1–10
21. Ashby G, Bone G (2016) Improved hybrid pneumatic-electric actuator for robot arms. in 2016 IEEE International Conference on Advanced Intelligent Mechatronics (AIM). Banff, Alberta, Canada
22. Manuello Bertetto A, Mazza L, Orrù PF (2015) Contact pressure distribution in guide bearings for pneumatic actuators. Exp Tech 39(2):46–54
23. Belforte G, Ivanov A, Manuello Bertetto A, Mazza L (2013) Experimental method for investigating air leakage in rodless cylinders. Exp Tech, p. 1–10
24. Falcão Carneiro J, Gomes de Almeida F. Experimental characteristics of a linear peristaltic actuator. in IFK 2018, 11th International Fluid Power Conference 2018. Aachen

25. Falcão Carneiro J, Gomes Almeida F (2018) Friction characteristics and servo control of a linear peristaltic actuator. Int J Adv Manuf Technol 96(5–8):2117–2126
26. DexyFlex. *FIRE TYANA SL*. [cited 06/02/2018]; Available from: https://dexyflex.eu/en/hoses/agro-assemblies/water-hoses-agro/tyana-sl-agro-hose/
27. Fitt. *Hiflat LD*. [cited 30/04/2018]; Available from: https://www.fitt.com/wp-content/uploads/2017/08/HIFLAT-LD_ITA-FRA-min.pdf
28. Productos Mesa. *FLEXIGOM (R) AIR*. [cited 06/02/2018]; Available from: https://productosmesa.com/flexigomr-air
29. Gent AN (1958) On the relation between indentation hardness and Young's modulus. Rubber Chem Technol 31(4):896–906
30. Falcão Carneiro J, Gomes Almeida F (2014) LuGre friction model: application to a pneumatic actuated system. in Controlo 2014, 11th Conference on Automatic Control. Porto, Portugal
31. SMC Corporation. *Pneumatic actuators*. [cited 30/04/2018]; Available from: https://www.smcworld.com/doc/smc/catalog/2008/e/webcatalog/p-guide/pages/Sentei_2_actuator.pdf
32. Festo. *Standard drives*. [cited 06/02/2018]; 3]. Available from: https://www.festo.com/net/SupportPortal/Files/17217/Standardantriebe_en.pdf